J. Fluid Mech. (2009), *vol.* 628, *pp.* 229–239.
doi:10.1017/S0022112009006636 Printed in the United Kingdom

Inside the moving layer of a sheared granular bed

H. MOUILLERON, F. CHARRU† AND O. EIFF

Institut de Mécanique des Fluides de Toulouse, Université de Toulouse,
2, Allée C. Soula, 31400 Toulouse, France

(Received 22 December 2008 and in revised form 11 February 2009)

The moving layer at the surface of a granular bed sheared by a viscous flow has been investigated experimentally. The fluid and particle velocities have been measured using particle imaging velocimetry (PIV) and particle tracking, respectively, with a technique of matched index of refraction. The mean velocity profiles are found to be parabolic. The models of Bagnold (*Phil. Trans. R. Soc. Lond.* A, vol. 249, 1956, pp. 235–297) and Leighton & Acrivos (*Chem. Engng Sci.*, vol. 41, 1986, pp. 1377–1384) fail to account for the observations. A simplified model assuming uniform particle concentration provides good agreement close to the threshold.

1. Introduction

Sand transport by rivers or tidal currents raises important issues in geophysics and civil engineering, such as erosion and dune formation. Similar issues also arise in multiphase flows in pipes, as in the petroleum or food industry. The fluid flow is often turbulent, but viscous flows are encountered in situations of increasing importance, such as heavy oil transportation in pipes. The present paper aims at a better understanding of particle transport in viscous flow, when the moving particles form a thin layer at the bed surface.

Several semi-empirical relationships have been proposed for the particle flux per unit width Q as a function of the bed shear-stress τ. For turbulent flow, these relationships are typically power laws with exponents close to 3/2 and numerical coefficients increasing slightly with the shear stress (Ribberink 1998). These laws unfortunately predict quite different transport rates near the threshold of particle motion, and the physical mechanisms at work remain unclear. Experimental data exhibit large scatter, in particular near the threshold which is itself not accurately defined (Buffington & Montgomery 1997). Detailed measurements of velocity and surface density of moving particles have been performed by Fernandez Luque & van Beek (1976), showing that the surface-averaged velocity $\overline{U}_p$ scales with the friction velocity $u_\tau = \sqrt{\tau/\rho}$ and that the surface density N_p scales with τ. The resulting flux is $Q = N_p\overline{U}_p \propto \tau^{3/2}$, in qualitative agreement with theoretical analyses by Bagnold (1973) and Engelund & Fredsoe (1976). No measurements are available on the internal structure of the moving layer.

For viscous flow, Bagnold (1956) and Leighton & Acrivos (1986) predicted $Q \propto \tau^3$ far from the threshold. The experiments of Charru, Mouilleron & Eiff (2004) showed that close to the threshold the exponent is 2 rather than 3, with surface density $N_p \propto \tau$, as for turbulent flow, and particle velocity $\overline{U}_p \propto \tau$. This study was limited

† Email address for correspondence: francois.charru@imft.fr

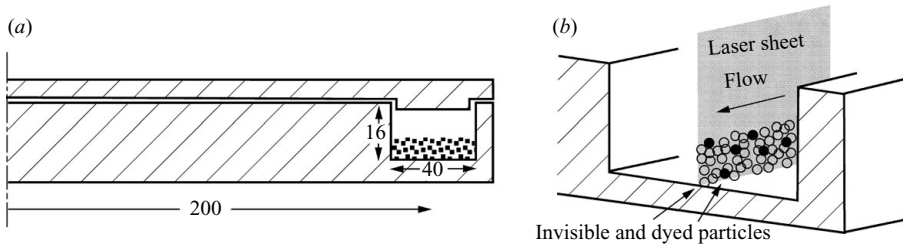

FIGURE 1. (*a*) Half cross-section of the annular channel (units in mm); (*b*) measurement plane.

to the observation of the bed surface viewed from above, which cannot provide any description of the internal structure of the moving layer. In a recent paper, Lobkovsky *et al.* (2008) provided an experimental study of the threshold shear stress and particle flux, finding a power law with an exponent close to 1.75; although one velocity profile and one concentration profile were provided, with low spatial resolution, they were not discussed.

In this paper, we report experiments aiming at a better understanding of the dynamics of the moving layer, from measurements of velocity profiles of the fluid and the particles, using a technique of matched refraction index. Experiments are conducted in a viscous flow which allows a thorough investigation and comparison with models. Section 2 describes the experimental set-up and the measurement techniques. The results are presented in § 3 and discussed in § 4.

2. Experimental set-up

The experiments have been performed in an annular Plexiglas channel of mean radius of 200 mm and rectangular cross-section $\Delta R \times H = 40 \times 16\,\mathrm{mm}^2$ (figure 1*a*). The rotation of the upper plate creates a Couette flow which drags the particle bed. The annular geometry was chosen to be able to study the long-time evolution and avoid problems associated with the supply of fluid and particles in open-ended rectilinear configurations.

In order to measure the velocities of both the fluid and the grains in the moving layer, their indices of refraction n were matched. The fluid chosen is a mixture of two plasticizing fluids (Santicizer 97 and 148) with $n = 1.446$ and $n = 1.506$, below and above that of acrylic grains with $n = 1.49$, density $\rho_p = 1180\,\mathrm{kg\,m^{-3}}$ and median diameter $d = 0.50\,\mathrm{mm}$. Particles were sieved and the distribution of diameters was controlled using a granulometer (Mastersizer, Malvern), giving $d_{10} = 0.41\,\mathrm{mm}$, $d_{50} = 0.50\,\mathrm{mm}$, $d_{90} = 0.60\,\mathrm{mm}$. The final mixture ($\rho = 1035\,\mathrm{kg\,m^{-3}}$, $\mu = 0.0218\,\mathrm{Pa\,s}$) was adjusted by including grains and analysing images taken in the measurement configuration. Although an almost perfect match was achieved, small air bubbles trapped within the acrylic grains during their manufacturing process led to a certain amount of residual diffused light. To track the particles in the moving bed, 8 % were rendered visible again by staining with cationic fluorescent dye (Astrazon Brilliant Red 4G 200 from DyStar Textilfarben), emitting in orange when excited by the green laser wavelength. This permitted an optical high-pass filter to be used to remove unwanted laser light.

The fluid phase was measured with a particle imaging velocimetry (PIV) technique, whereas the grain phase was measured separately via particle tracking, with the same

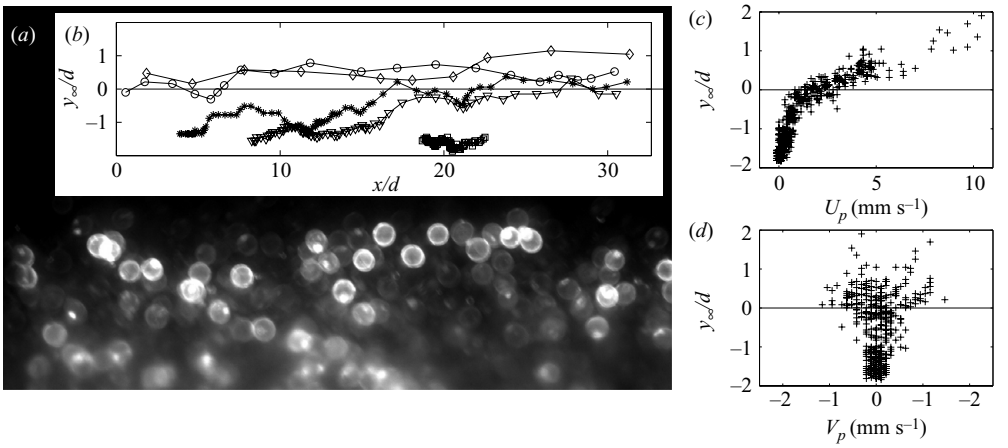

FIGURE 2. (*a*) Sample image of the particles inside the bed obtained with the index-matching technique, with $d = 0.5$ mm; (*b*) typical particle trajectories with $\delta t = 0.25$ s. (*c*), (*d*) Velocities U_p and V_p of individual particles; $\theta = 0.67$, 13 particles tracked, 423 data points.

laser and camera set-up. The PIV technique requires the addition of small seeding particles, here 10 μm hollow glass spheres of density 1110 kg m^{-3}. A 2 mm thick vertical laser sheet generated by a 30 mJ Nd:Yag double-pulse laser was positioned in the centre of the channel (figure 1*b*) from above. A 1280×1024 px 12-bit CCD camera with a 105 mm Nikon macro lens was used to capture the images of width 16 mm corresponding to spatial resolution of 78 px mm^{-1}. For the PIV measurements, five image pairs were acquired at 0.8 Hz with a PIV time interval adjusted to have a maximum displacement of about 15 px. For the particle-tracking images, the image acquisition frequency varied from 1 Hz to 4 Hz to optimize the tracking between 100 and 200 consecutive images.

The PIV images were processed with the software developed by Fincham & Spedding (1997), with resolution of the velocity field of about $d/2$. The grain phase was manually masked so that PIV displacements were only computed for the fluid phase. The five velocity fields acquired yielded a total of 200 velocity profiles, which were then averaged. The particles were manually tracked in the image series (see figure 2*a*) with the Optimas software to compute and store the position of the centroid of the particles (see Mouilleron 2002 for more details).

The experimental procedure consisted of first levelling the bed of particles by resuspending the bed at high velocity and then stopping the flow. Particles settled, forming a loose flat bed. The experiments were started at the lowest flow velocity, and measurements were begun after bed equilibrium was reached, with reproducible threshold Shields number $\theta_t = 0.12$. (See Charru *et al.* 2004 for a discussion of the armouring process leading to the bed at equilibrium.) The typical fluid thickness was $h = 7$ mm, and the maximum upper plate velocity at the mean radius was $U_w = 0.158$ m s^{-1} corresponding to shear rate $\gamma = U_w/h = 23$ s^{-1}. The corresponding flow Reynolds number $Re = \rho U_w h/\mu$ was 60, with negligible secondary flow due to centrifugal forces (Charru *et al.* 2004). The bed shear stress is measured by the Shields number

$$\theta = \frac{\mu\gamma}{(\rho_p - \rho)gd}. \tag{2.1}$$

Its maximum value was 0.67, with corresponding particle Reynolds number $Re_p = \rho\gamma d^2/\mu = 0.24$. Finally, the sedimentation Reynolds number $Re_s = \rho U_S d/\mu$ was 0.022, with Stokes settling velocity $U_S = (\rho_p - \rho_f)gd^2/18\mu = 0.92\,\mathrm{mm\,s^{-1}}$.

3. Results

For small upper plate velocity U_w, corresponding to Shields numbers θ lower than the threshold $\theta_t = 0.12$, no particle motion was observed. For increasing U_w, particles near the bed surface began to move. For each θ, the number of tracked particles was between 11 and 14 and the number of recorded positions between 362 and 553. Typical trajectories are shown in figure 2(b) for $\theta = 0.67$. The upper particles quickly cross the field of view, whereas deeper particles move very slowly. For the reference level of the vertical position, a natural choice would be the bed surface at rest. However, this level is not easy to define and measure with a desired accuracy of $d/10 = 0.05\,\mathrm{mm}$. Moreover, this level slowly decreased during the experiment, by about one particle diameter per hour, due to the slow secondary flow which causes the particles to drift towards the inner sidewall of the channel. Thus, a more suitable reference was found to be the level at which the linear fluid velocity profile above the bed, as measured by PIV, extrapolates to zero by linear regression from the upper plate down to the moving layer. The accuracy of this reference level was estimated to be $d/20$. The vertical position y_∞ is defined from this level.

From the successive positions of the tracked particles, their longitudinal and vertical velocities U_p and V_p were calculated from a first-order finite-difference scheme. Figure 2(c,d) displays all the measured U_p and V_p for $\theta = 0.67$. It can be seen that the thickness of the moving layer is about $3d$ and that U_p is of a few millimetres per second with large dispersion due to particle interactions; V_p is smaller by a factor of about 10, with zero mean value as expected and the largest dispersion arising close to $y_\infty = 0$.

From the velocities U_p of individual particles, the mean value u_p in bands of vertical thickness $d/3$ was calculated. Figure 3(a) displays the mean velocity profiles for six values of θ increasing from 0.20 to 0.67, normalized with U_S. For clarity, the profiles for increasing θ have been shifted to the right by U_S. It appears that higher θ corresponds to larger mean velocity and larger thickness of the moving layer, as expected. However, the interface between the fixed bed and the moving layer is not sharp. Figure 3(b) displays the same profiles, each normalized with its characteristic velocity γd. It can be seen that this simple scaling provides a good collapse of the data points.

In order to check the consistency of the present measurements with those of Charru *et al.* (2004) obtained by tracking the particles as viewed from above (without index matching), an averaged velocity $\overline{U}_p = \sum_i U_{p,i}/N$ was computed over the N-measured U_p, for each θ. Once divided by γd, this velocity was found to be a constant for $\theta \leqslant 0.52$, $\overline{U}_p/\gamma d = 0.11 \pm 0.02$, with no well-defined trend with θ. (A higher value of 0.16 was found for $\theta = 0.67$.) This result agrees with Charru *et al.* (2004) who found $\overline{U}_p = 0.10\,\gamma d$.

Figure 3(b) also shows, in the inset, the fluid velocity u_f, normalized with the characteristic velocity γd. Since all the profiles collapse on the same line in the bulk of the flow due to the definition of the reference level, as was verified, only the region close to the moving layer is shown in the figure. In this region, fluid velocity profiles are curved due to interactions with the particles. Although the normalized profiles appear nearly superposed, the depth at which the fluid velocity vanishes increases with θ.

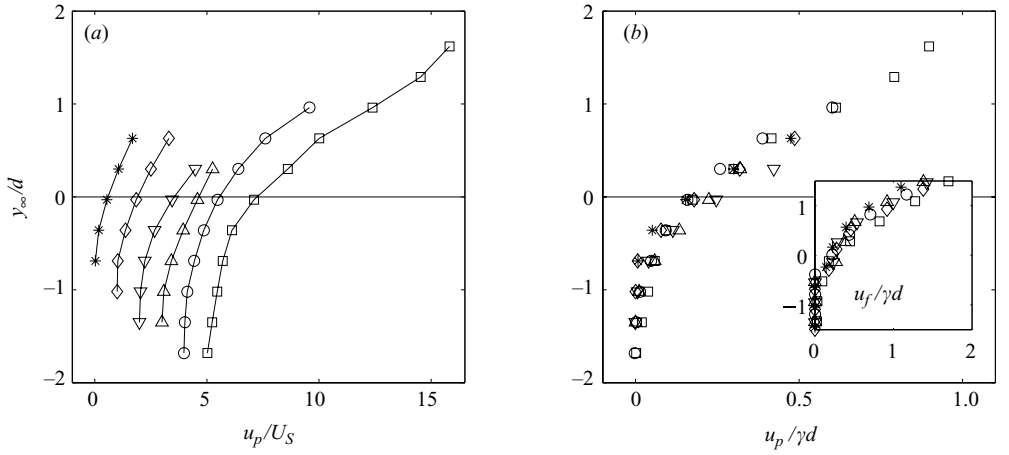

FIGURE 3. (*a*) Profiles of u_p/U_S for $\theta = 0.20$, 0.26, 0.33, 0.39, 0.52 and 0.67, from left to right, shifted horizontally by U_S for clarity; (*b*) $u_p/\gamma d$ for the same θ. Inset: fluid velocity $u_f/\gamma d$ in the region $-1.5 < y_\infty/d < 1.5$.

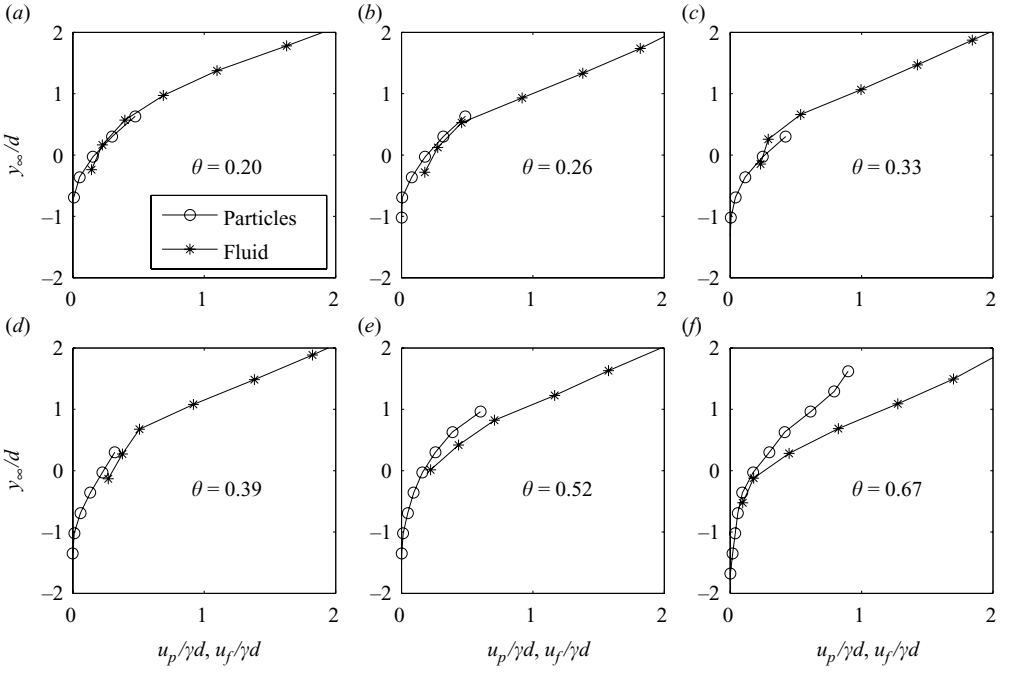

FIGURE 4. Particle and fluid velocity profiles inside the moving layer, for six Shields numbers.

The particle and fluid velocities are plotted on the same plots in figure 4, for each θ. It appears that for $\theta < 0.5$ (figure 4*a–d*), the fluid and particle velocities in the moving layer are equal, with no significant slip velocity. However, for $\theta > 0.5$, the fluid velocity in the moving layer is higher than that of the particles. This slip velocity increases with θ, the fluid velocity being about twice that of the particles for the highest $\theta = 0.67$.

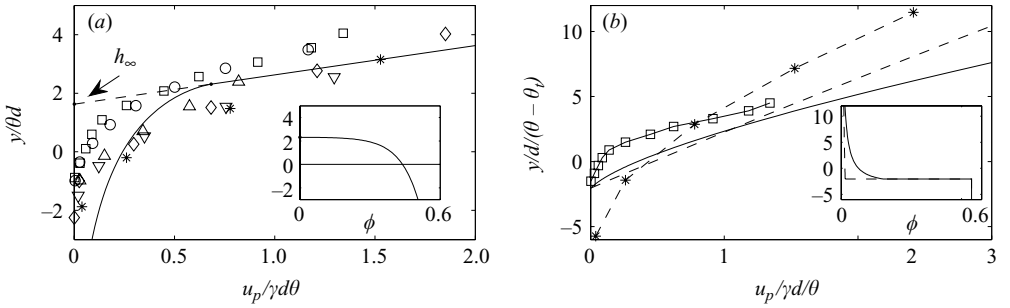

FIGURE 5. (*a*) Velocity profile from Leighton & Acrivos (1986) and particle velocity measurements for all θ (same markers as in figure 3); inset: concentration profiles; $\phi_0 = 0.6$. (*b*) Velocity profiles from Bagnold (1956) and measurements, for $\theta/\theta_t = 0.20$ (- -) and 0.67 (—); inset: concentration profiles; $\theta_t = 0.12$, $\phi_0 = 0.6$. The origin of the y-axis is the bed at rest.

4. Analysis

In this section, the measurements are compared to the models of Bagnold (1956) and Leighton & Acrivos (1986) and then to a simplified version of Bagnold's (1956) model.

4.1. *Viscous resuspension model of Leighton & Acrivos (1986)*

The viscous resuspension theory of Leighton & Acrivos (1986) assumes particles without inertia which follow the fluid with the same velocity. The particle concentration ϕ results from an equilibrium between downward sedimentation and upward diffusion induced by the gradient $\partial_y\phi$ of the particle concentration. The sedimentation flux is $f(\phi)\,U_S\,\phi$, where U_S is the Stokes settling velocity of a single particle and $f(\phi) < 1$ is the 'hindrance function' taking into account the retarding effect of the other particles. The shear-induced diffusion flux is written as $(\tau/\mu_f\mu)(d^2/4)\,D\,\partial_y\phi$, where $\mu_f(\phi)$ is the relative effective viscosity; $\tau/\mu_f\mu$ is the local shear rate; and $D(\phi) = O(1)$ is a dimensionless diffusion coefficient. Finally, $f(\phi)$, $\mu_f(\phi)$ and $D(\phi)$ are given by empirical relations (see Leighton & Acrivos 1986). The origin of the vertical y-axis is set at the location of the interface at rest. By integrating the mass balance from the bottom of the moving layer at $y = -h_b$ at which the concentration is ϕ_0, the height y at which the volume concentration is ϕ is found to be

$$\frac{y + h_b}{d} = \frac{9\theta}{2}\int_\phi^{\phi_0} \frac{D}{\phi\, f\, \mu_f}\,\mathrm{d}\phi. \tag{4.1}$$

Defining the upper bound $y = h_m$ of the moving layer as the location at which the concentration ϕ vanishes, the thicknesses h_b and h_m are found to be proportional to the Shields number, $h_b/d = 11.8\,\theta$ and $h_m/d = 1.86\,\theta$.

By integrating the x-momentum conservation equation with the boundary condition $u(-h_b) = 0$, the velocity u at which the concentration is ϕ is found to be

$$\frac{u}{U_S} = 4\left(\frac{9\theta}{2}\right)^2 \int_\phi^{\phi_0} \frac{D}{\phi\, f\, \mu_f^2}\,\mathrm{d}\phi. \tag{4.2}$$

Finally, numerical integration of (4.1) and (4.2) defines the velocity profile $u(y)$ through the parameter ϕ.

Figure 5(*a*) displays the velocity profile (4.2) with the measured velocity points, for all θ. It also shows in the inset the concentration profile for which there are no measurements. For comparison with the model, the origin of the vertical axis y_∞

used in the experiments had to be shifted to the bed at rest, using the relationship $y - y_\infty = h_\infty$, where the height h_∞ is found from the model to be $h_\infty = 1.63\,\theta d$ (see figure 5*a*). It can be seen that the data points do not fall well on the theoretical curve and that their scatter is even larger than that displayed in figure 3(*b*) with the simple scaling γd. Choosing the Krieger–Dougherty viscosity $\mu_f = (1 - \phi/\phi_0)^{-2.5\phi_0}$ leads to a slightly different velocity profile, but the agreement with the experiments remains poor.

4.2. *Bagnold's (1956) model*

Bagnold's theory (Bagnold 1956) on sediment transport by viscous flow is based on experiments he performed on suspensions of neutrally buoyant particles sheared in an annular Couette flow (Bagnold 1954). By considering that the shear stress τ is the sum of a fluid shear stress τ_f transmitted by the fluid and a particle shear stress τ_p corresponding to encounters between particles and assuming that the fluid behaves as a Newtonian fluid with effective viscosity given by Einstein's law, these experiments showed that, in the viscous regime which is relevant here, τ_p is given by

$$\tau_p = \mu_p(\phi)\,\mu \frac{\mathrm{d}u_p}{\mathrm{d}y}, \quad \mu_p(\phi) = 2.2\,\lambda^{3/2}, \tag{4.3}$$

where λ is a linear particle concentration related to ϕ by $1/\lambda = (\phi_0/\phi)^{1/3} - 1$. From pressure measurements, Bagnold (1954) also found that the normal stress p_p due to particle interactions is related to the shear stress τ_p by a Coulomb-type friction law, $\tau_p/p_p = \tan\alpha$, where the dynamic friction coefficient is $\tan\alpha = 0.75$ in the viscous regime. Note that although these experiments have been criticized by Hunt *et al.* (2002), they have not been repeated up to now.

In his analysis of a granular bed sheared by a viscous flow, Bagnold (1956) assumes that the above results are still valid for heavy particles with strong concentration and velocity gradients normal to the bed. For such a flow, the normal particle stress p_p at the vertical level y is the apparent weight per unit surface of the particles above that level. Penetrating deeper into the moving layer, τ_p increases due to the increasing granular pressure p_p, so that τ_f decreases; the lower bound of the moving layer, say at $y = -h_b$ with the origin of the y-axis at the bed surface at rest, is assumed to correspond to τ_f being reduced to the threshold τ_t. With this 'Bagnold's hypothesis', h_b is given by $h_b/d = (\theta - \theta_t)/\phi_0 \tan\alpha$. Then, the concentration profile $\phi(Y)$ can be obtained from

$$\tan\alpha \int_{-h_b/d}^{Y} \phi(Y)\,\mathrm{d}Y = \frac{\mu_f(\phi)}{\mu_f(\phi) + \mu_p(\phi)}\,\theta - \theta_t, \quad Y = y/d. \tag{4.4}$$

In particular, this equation gives the particle concentration just above the bed surface $Y = 0$, lower than ϕ_0. Neglecting any slip between the fluid and particles and assuming that the velocity vanishes at $y = -h_b$, the velocity profile is

$$\frac{u_p}{U_S} = \frac{u_f}{U_S} = 18\,\theta \int_{-h_b/d}^{Y} \frac{\mathrm{d}Y}{\mu_f(\phi) + \mu_p(\phi)}. \tag{4.5}$$

Figure 5(*b*) displays the velocity profiles for the lowest and highest Shields numbers of the experiments, $\theta = 0.20$ and 0.67, with $\theta_t = 0.12$ (Ouriemi *et al.* 2007); the concentration profiles are shown in the inset. First, it can be observed that different θ lead to different profiles, unlike the viscous resuspension theory which ignores the threshold θ_t. Also in contrast with the viscous resuspension theory, the particle concentration decreases slowly with height, as $\phi \sim \theta/y^2$, so that the velocity gradient

reaches that of the pure fluid at large distances. Figure 5(*b*) also displays the measured particle velocity for the same two Shields numbers. The major trend is that Bagnold's model overestimates the particle velocity; the same conclusion is true for the intermediate θ, not shown in the figure for clarity.

4.3. *Simplified Bagnold's model*

Agreement between observations and the above models could be improved by refining the empirical closure laws; in particular, refining $\mu_p(\phi)$ in Bagnold's model could avoid the slow decrease of the particle concentration $\phi(y)$ and make it zero at some finite height h_m above the fixed bed. In the absence of theoretical argument for such refinements, a simple way is attempted here by assuming a uniform concentration ϕ. Then, the fluid shear stress is found to be

$$\tau_f = \tau - p_p \tan\alpha \qquad \text{with} \quad p_p = \phi(\rho_p - \rho_f) g (h_m - y). \tag{4.6}$$

We consider that the location $y = -h_b$ at which the velocity vanishes corresponds to the fluid shear stress being reduced to zero (rather than τ_t; see Seminara, Solari & Parker 2002 for a criticism of the Bagnold hypothesis). With the mass conservation equation $h_b\phi_0 = (h_m + h_b)\phi$, the lower and upper limits of the moving layer are then found to be $h_b/d = \theta/(\phi_0 \tan\alpha)$ and $(h_m + h_b)/d = \theta/(\phi \tan\alpha)$.

The fluid velocity profile is obtained from the momentum equation $\mathrm{d}u_f/\mathrm{d}y = \tau_f/\mu_f\mu$, as the quadratic relation

$$\frac{u_f}{U_S} = \frac{9\phi \tan\alpha}{\mu_f} \left(\frac{y + h_b}{d}\right)^2. \tag{4.7}$$

This equation requires some numerical values for the parameters. For the friction coefficient, the value $\tan\alpha = 0.75$ found by Bagnold (1954) for viscous flow can still be used. Another close estimation can be obtained from Cassar, Nicolas & Pouliquen (2005), who propose, from their experiments on avalanches, a law for the friction coefficient as a function of a parameter I. This parameter is the ratio of a characteristic falling time of a particle, here d/U_S, and the flow time scale γ^{-1}; thus $I = 18\theta$ which here is larger than 2 and gives a friction coefficient between 0.7 and 0.8. The maximum particle concentration is taken as $\phi_0 = 0.6$ as previously. The concentration ϕ can be deduced from measurements of the thickness of the moving layer via the equation $(h_b + h_m)/d = \theta/(\phi \tan\alpha)$. This thickness was estimated from the lower and upper positions of the moving particles and found to increase linearly with θ according to $(h_b + h_m)/d \approx 5\theta$. Comparison of these two relations for $(h_b + h_m)/d$ gives $\phi \approx 0.27$. Finally, the viscosity was deduced with the Krieger–Dougherty correlation $\mu_f = (1 - \phi/\phi_0)^{-2.5\phi_0}$, giving $\mu_f = 2.45$.

For the particle velocity u_p, several corrections to the fluid velocity (4.7) might be introduced. The first correction should take into account the threshold $\theta_t = 0.12$; its order of magnitude is the fluid velocity at the height at which $\tau_f = \tau_t$; this height y_t is found from the model to be $y_t + h_b = 0.53d$, with corresponding fluid velocity $0.33U_S$. A second correction is due to the curvature of the fluid velocity profile (Faxen), which gives an overspeed of a fraction of U_S. A third correction arises from the stresses transmitted to the fixed bed through long chains of contacts between the particles (Darcy); with the classical permeability $K = (1 - \phi)^3 d^2/180\phi^2$, this correction is also found to be a fraction of U_S. Finally, an inertial correction should be introduced, accounting for small particle inertia. (In the present experiments, the particle Reynolds number Re_p is in the range 0.1–0.3.) Due to the uncertain modelling of these corrections and since the above estimations show that they would be of a

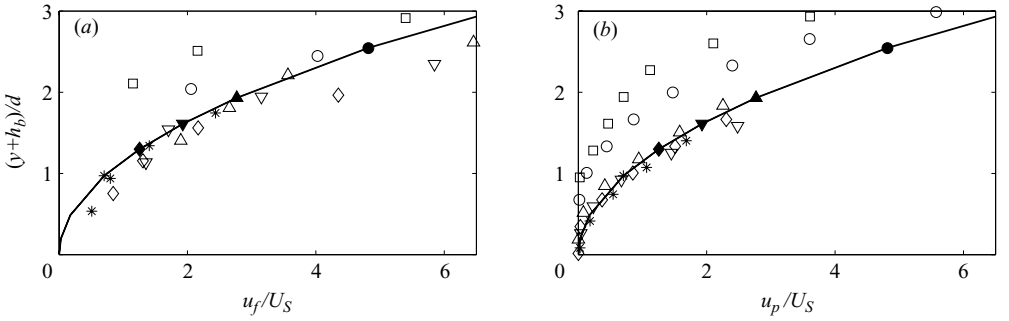

FIGURE 6. (*a*) Fluid velocity and (*b*) particle velocity, for all θ with the same markers as in figure 3; in both plots the continuous line is the prediction (4.7) with solid markers at the predicted upper surface of the moving layer h_m, for each θ; $\phi_0 = 0.6$, $\phi = 0.27$, $\tan\alpha = 0.75$.

fraction of U_S, the particle velocity is here considered equal to that of the fluid, i.e. $u_p(y) = u_f(y)$; this approximation is consistent with the observations reported in the previous section, at least for $\theta < 0.5$. Finally, the measured particle velocity will be compared in the following to the velocity (4.7).

Figure 6(*a*) displays the measured fluid velocity for all θ, as a function of the distance $y + h_b$ to the lower bound of the moving layer (with the measured vertical positions y_∞ shifted by $y - y_\infty = h_\infty$, where h_∞ was calculated from the model). The continuous line is the fluid velocity prediction (4.7) with the parameter values given above; the filled markers correspond to the predicted upper bounds $h_m(\theta)$ of the moving layer, each marker being identical to the open ones for the measured velocities at the same θ. It can be seen that for $\theta < 0.5$ the velocity points fall close to the predicted curve, with scatter probably related to the difficulties of performing PIV in between particles. However, for the two highest Shields numbers $\theta = 0.52$ (○) and $\theta = 0.67$ (□), the measured points are significantly above the predicted velocity. Figure 6(*b*) displays the particle velocity with the same scales and comparison with the same velocity prediction (4.7). It can be seen that for $\theta < 0.5$, the measured velocities collapse on the theoretical prediction, with quite a small scatter. However, the data points for $\theta = 0.52$ and $\theta = 0.67$ fall again significantly above; the discrepancy is clearly related to the slip velocity between the fluid and particles as shown in figure 4. Finally, it can be noted that taking Einstein's law instead of the Krieger–Dougherty correlation for the viscosity, or varying the particle concentration in the range 0.25–0.30, changes little the agreement between measurements and the theoretical prediction (4.7).

5. Summary and discussion

Measurements have been presented of both the particle and fluid velocities, u_p and u_f, within the moving layer of a granular bed sheared by a viscous flow (particle Reynolds number $Re_p < 0.3$). Once normalized with the characteristic velocity γd, a reasonable collapse of the parabolic profiles was found in the explored range of Shields number, $\theta \leqslant 0.67$. The thickness of the moving layer was found to be approximately equal to $5\theta d$. For $\theta < 0.5 \approx 4\theta_t$, the fluid and particle velocities are equal. For $\theta > 0.5$, a significant slip velocity is visible.

Measurements were then compared to the resuspension model of Leighton & Acrivos (1986) and the model of Bagnold (1956). Neither of these models provides good predictions. It was noted that the friction coefficient found by Bagnold (1954)

for viscous flow, $\tan\alpha = 0.75$, is very close to that deduced from the analysis of Cassar *et al.* (2005) of their experiments on avalanches. A modification of Bagnold's model was then proposed, which assumes uniform particle concentration ϕ. The great advantage of this assumption is that it provides an explicit quadratic relationship for the fluid velocity $u_f(y)$, as a function of the distance $y + h_b$ to the fixed bed. A discussion was then given of four corrections for the particle velocity $u_p(y)$, arising from the threshold, Faxen, Darcy and inertia effects, with the conclusion that these corrections should be small, so that $u_p = u_f$ at the dominant order. With the mean particle concentration $\phi = 0.27 \approx (1/2)\phi_0$ deduced from the experiments, the measured velocity profiles collapse on the predicted curve for all $\theta < 0.5 \approx 4\theta_t$, with no adjustable parameter. Beyond this range, the model overpredicts the fluid and particle velocity, a failure which is likely to be related to the observed appearance of significant slip velocity.

An important practical question is that of the particle flux Q, which involves both the particle velocity and concentration. Integration of the velocity profile with uniform $\phi = (1/2)\phi_0$ gives $Q/U_S d = 10.2\,\theta^3$; this result is similar to that of Leighton & Acrivos (1986) which gives the same scaling with a lower coefficient of 7.5; Bagnold's model also predicts the same scaling with θ, but the flux diverges logarithmically with height due to the slow decrease of the concentration ($u \sim y$, $\phi \sim y^{-2}$). However, the above result is likely to overpredict the actual flow rate, since the high velocity in the upper part of the moving layer is actually associated with ϕ much smaller than the assumed uniform value. Indeed, with the surface density of moving particles $N_p d^2 = 0.47(\theta - \theta_t)$ found by Charru *et al.* (2004), the concentration of a monolayer of moving particles is $\phi = 0.03$ for a typical $\theta = 2\theta_t = 0.24$; this concentration is one order of magnitude smaller than the value considered here. Finally, the particle flux found by Charru *et al.* (2004) $Q/U_S d = 0.44\,\theta(\theta - \theta_t)$ is expected to provide better prediction, at least for $\theta < 0.5$, than the cubic power law.

In conclusion, particle and fluid velocity measurements in the moving layer have been understood with a model which predicts the right profiles close to the threshold ($\theta < 0.5$). The development of a more general model requires a better knowledge of fluid–particle interactions. For that, measurements of the particle concentration are needed, together with an analysis of the velocity fluctuations. A related open question is that of the relaxation time or length scale associated with time-varying or space-varying flows. These questions merit further investigation.

We would like to acknowledge E. J. Hinch for fruitful suggestions and enlightening comments. We also thank S. Cazin for his valuable technical help for the measurements.

REFERENCES

Bagnold, R. A. 1954 Experiments on a gravity-free dispersion of large solid spheres in a Newtonian fluid under shear. *Proc. R. Soc. Lond.* A **225**, 49–63.

Bagnold, R. A. 1956 The flow of cohesionless grains in fluids. *Phil. Trans. R. Soc. Lond. A* **249**, 235–297.

Bagnold, R. A. 1973 The nature of saltation and of 'bed-load' transport in water. *Proc. R. Soc. Lond.* A **332**, 473–504.

Buffington, J. M. & Montgomery, D. R. 1997 A systematic analysis of eight decades of incipient motion studies, with special reference to gravel-bedded rivers. *Water Resour. Res.* **33**, 1993–2029.

Cassar, C., Nicolas, M. & Pouliquen, O. 2005 Submarine granular flows down inclined planes. *Phys. Fluids* **17**, 103301.

Charru, F., Mouilleron, H. & Eiff, O. 2004 Erosion and deposition of particles on a bed sheared by a viscous flow. *J. Fluid Mech.* **519**, 55–80.

Engelund, F. & Fredsøe, J. 1976 A sediment transport model for straight alluvial channels. *Nordic Hydrol.* **7**, 293–306.

Fernandez Luque, R. & van Beek, R. 1976 Erosion and transport of bedload sediment. *J. Hydraul. Res.* **14**, 127–144.

Fincham, A. M. & Spedding, G. R. 1997 Low cost, high resolution DPIV for measurement in turbulent fluid flows. *Exp. Fluids* **23**, 449–462.

Hunt, M. L., Zenit, R., Campbell, C. S. & Brennen, C. E. 2002 Revisiting the 1954 suspension experiments of R. A. Bagnold. *J. Fluid Mech.* **452**, 1–24.

Leighton, D. & Acrivos, A. 1986 Viscous resuspension. *Chem. Engng Sci.* **41**, 1377–1384.

Lobkovsky, A. E., Orpe, A. V., Molloy, R., Kudrolli, A. & Rothman, D. H. 2008 Erosion of a granular bed driven by laminar fluid flow. *J. Fluid Mech.* **605**, 47–58.

Mouilleron, H. 2002 Instabilités d'un milieu granulaire cisaillé par un fluide. Doctorate thesis, Université Paul Sabatier.

Ouriemi, M., Aussillous, P., Medale, M., Peysson, Y. & Guazzelli, E. 2007 Determination of the critical Shields number for particle erosion in laminar flow. *Phys. Fluids* **19**, 061706.

Ribberink, J. S. 1998 Bed-load transport for steady flows and unsteady oscillatory flows. *Coastal Engng* **34**, 59–82.

Seminara, G., Solari, L. & Parker, G. 2002 Bed load at low Shields stress on arbitrarily sloping beds: failure of the Bagnold hypothesis. *Water Resour. Res.* **38**, 1249.